Turkish Journal of Engineering

https://dergipark.org.tr/en/pub/tuje

e-ISSN 2587-1366

Multivariable generalized predictive control of reactive distillation column process for biodiesel production

Mehmet Tuncay Çağatay[*1], **Süleyman Karacan** [2]

[1]*Ministry of National Defence, Presidency of General Staff, Ankara, Turkey*
[2]*Ankara University, Engineering Faculty, Department of Chemical Engineering, Ankara, Turkey*

Keywords
Multivariable Generalized Predictive Control
PID Control
Reactive Distillation Column
Biodiesel

ABSTRACT

Most industrial control systems consist of a significant number of control loops. Generally, large processes are divided into many interconnected subsystems affecting each other, thus creating multivariable systems known as multiple–input multiple–output (MIMO) process. Generalized Predictive Control (GPC) based control algorithm is most suitable for MIMO systems. In this study, multivariate nonlinear (NL) GPC and discrete–time PID control of calcium oxide catalyst–packed reactive distillation (RD) column used for biodiesel production from waste cooking oil were investigated. Temperatures of reaction and reboiler sections were controlled by using non–decoupled and decoupled MIMO NLGPC and discrete–time MIMO PID algorithms. Feed flow rate with constant molar ratio and reboiler heat duty parameters were selected as manipulating variables. All recommended control methods, except for non-decoupled MIMO NLGPC, have been found to perform satisfactorily reference tracking and disturbance rejection in RD column. Consequently, the best control results were obtained in the decoupled MIMO NLGPC.

1. INTRODUCTION

In recent years, requirements for high quality process control have increased significantly in parallel to the growing complexity of plants and sharper specifications of product feature. But, smart and model–based control techniques have also been developed to accomplish strict control algorithms. On the other hand, computing power has increased to a very high level. Thus, computationally expensive computer models become appropriate to solve much complex problems.

The idea of the control strategy for a process is to maintain the desired operational variables smoothly and consistently. Thus, operating conditions of the system are fixed by control action to reach the target in the most effective way possible. When the process conditions change, the controllers need to be adjusted again to attain acceptable control results. Generalized Predictive Control (GPC) is considered as to be excellent to get satisfactory controls. This receding horizon method predicts the output of the plant in several sampling intervals, using assumptions about future control actions (Clarke et al. 1987). It is also possible by GPC to achieve stable control of process with variable dead–time and an instantaneously–changing model order, providing the sufficient input/output data for reasonable plant recognition. It is effective for a plant which is simultaneously open–loop unstable and nonminimum–phase and with over parameter, as well. To establish the GPC algorithm, it is necessary to use a linearized model in terms of ARIMAX form (Clarke and Mohtadi 1989).

In the literature, there are a few model structures proposed for the definition of the nonlinear systems. Volterra series and Block oriented models are some examples for nonlinear patterns. The nonlinear difference equation model, NARIMAX, known as the Nonlinear Auto Regressive Moving Average with Exogenous, provides a combined representation for a wide range of nonlinear systems. Namely, a general nonlinear input/output polynomial model is used to recognize the system. It is well known that system identification is one of the most important and time–consuming tasks regarding proper application. Several control approaches to nonlinear process have been

* **Corresponding Author**

*(mehmetcagatay71@gmail.com) ORCID ID 0000 – 0002 – 8625 – 8058
(karacan@eng.ankara.edu.tr) ORCID ID 0000 – 0001 – 8113 – 7874

Cite this article

Çağatay M T & Karacan S (2022). Multivariable Generalized Predictive Control of Reactive Distillation Column Process for Biodiesel Production. Turkish Journal of Engineering, 6(1), 40-53

Research Article / DOI: 10.31127/tuje.801441

Received: 28/09/2020; Accepted: 11/01/2021

developed and successfully applied to certain systems (Ahn et al. 1999; Chen and Xu 2001; Karacan 2003).

Some countries are looking for alternative methods to meet the need for an environmentally friendly and renewable fuel supply due to increased fuel demand and global concerns about the effects of greenhouse gases. Biodiesel is an alternative source to replace fossil diesel (Donato et al. 2009). It is produced by transesterification of long chain fatty acids (FA) derived from vegetable oils and animal fats with aliphatic alcohols in the presence of a suitable catalyst to form long chain fatty acid methyl ester (FAME) and glycerol (Srivastava and Prasad 2000).

Although there are many biodiesel production facilities in the world, the main technical challenge is how to make biodiesel profitable, given the high expense of crude vegetable oil used as a source of triglyceride. Economic evaluation results show that raw material price constitute a significant part of the total cost production. Using waste cooking oil (WCO) instead of virgin oil to produce biodiesel is a way to lower the charge since it is considered as to be about half price of the virgin oil (Kulkarni and Dalai 2006).

Transesterification reaction can be catalyzed by an acid, base, or enzymes. Homogeneous and heterogeneous alkali and acid catalysts have been studied (Zhang et al. 2003). Heterogeneous catalysts have advantages of effortlessly separation and regeneration techniques (Sharma et al. 2008). Heterogeneous basic catalysts include alkaline–earth metal oxides such as calcium oxide (CaO), MgO, SrO, and hydrotalcites (Kouzu et al. 2008). Being superior catalytic, easily accessible, and cheaper, CaO has been mentioned in a series of articles examining heterogeneous catalytic reaction for biodiesel synthesis (DiSerio et al. 2008).

Reactive separation is a process combining reaction and separation at the same time. It allows simultaneous production and removal of products in a single unit. Thus, it increases efficiency and selectivity, reduces energy consumption, eliminates the need for solvents, and leads to integrated high–efficiency systems. In the process, separation could be improved through reaction by overcoming azeotropes, removing contaminants. On the other hand, reactions could be enhanced by means of separation via increasing overall rates, overcoming equilibrium limitations, improving selectivity. So, maximum effect can be accomplished by considering both features simultaneously (Harmsen 2007).

Before synthesis in a real facility, it is very important to establish a prototype and simulate it using a process simulator such as Aspen HYSYS. Thus, it could be anticipated how its real–time production would be. There are several simulation studies on biodiesel production in a batch and continuous flow reactor system with a homogeneous alkali or acidic catalyst (Martín and Grossmann 2012). However, there are very few simulation studies on biodiesel production in the reactive distillation (RD) column. Çağatay and Karacan (2018) investigated the simulation and optimization of packed RD column utilized in the production of FAME. Biodiesel was procured by transesterification reaction between WCO and methanol in the presence of heterogeneous basic CaO catalysis. The simulation of CaO–packed RD column was designed by Aspen HYSYS and optimum values of the parameters were specified.

In this study, multivariate NLGPC, based on NARIMAX model, and discrete–time PID control, based on ARX model, were inspected in the temperature control of reaction, and reboiler sections of a CaO catalysis–packed RD column used for biodiesel synthesis from WCO. Before process control studies, PRBS signals and recursive system identification algorithms were utilized to estimate the polynomial parameters of NARIMAX and ARX models. Lastly, process control performances were compared.

2. METHOD

2.1. Materials

WCO was collected from local restaurants in Ankara, Turkey. Heterogenous basic CaO catalyst was employed in the biodiesel synthesis. Methanol and CaO were purchased from Sigma–Aldrich. The composition of WCO (see Table 1) was revealed by Perkin Elmer Clarus 500 model gas chromatography using Agilent HP–88 (100 m x 0.25 mm x 0.2 μm) capillary column and Flame Ionization Detector with helium as the carrier gas. Analysis was made according to "CoI/T.20/Doc.No.17, 2001" method acknowledged by International Olive Oil Council. The oven temperature was programmed at 175 °C for 12 min, and ramped to 225 °C at a rate of 2 °C/min for 12 min. In addition, the injector and detector temperatures were hold at 250 °C and 280 °C, in turn.

Table 1. FA composition (%w) and properties of WCO

Parameters	Value
palmitic	20.99
stearic	4.92
oleic	38.12
linoleic	29.73
water content	%0.09
acid value	1.09 (mg KOH/g oil)
color	golden yellow

Transesterification was carried out in a packed RD column demonstrated in Fig. 1 and 2. The column has a height of 1.2 m and a diameter of 0.05 m, excluding condenser and reboiler. It consisted of a cylindrical condenser with a diameter and height of 0.05 and 0.225 m, respectively. The column was partitioned into two subdivisions. The upper and lower sections were the reaction and stripping parts, in turn. The stripping unit was packed with Raschig rings, while the reaction division was filled with small lumps ~3–20 mm CaO solid catalysis and Raschig rings. The reboiler was spherical with a volume of 4 liters. WCO and methanol were fed to the column at the upper inlet. Condensed methanol at the condenser was totally recycled to the column.

Besides, all signal inputs of feed flow rate and reboiler heat duty, and signal outputs of temperatures of upper, reaction and lower units were implemented and measured on−line using MATLAB/Simulink, and input/output (I/O) modules connected to the equipment and computer system.

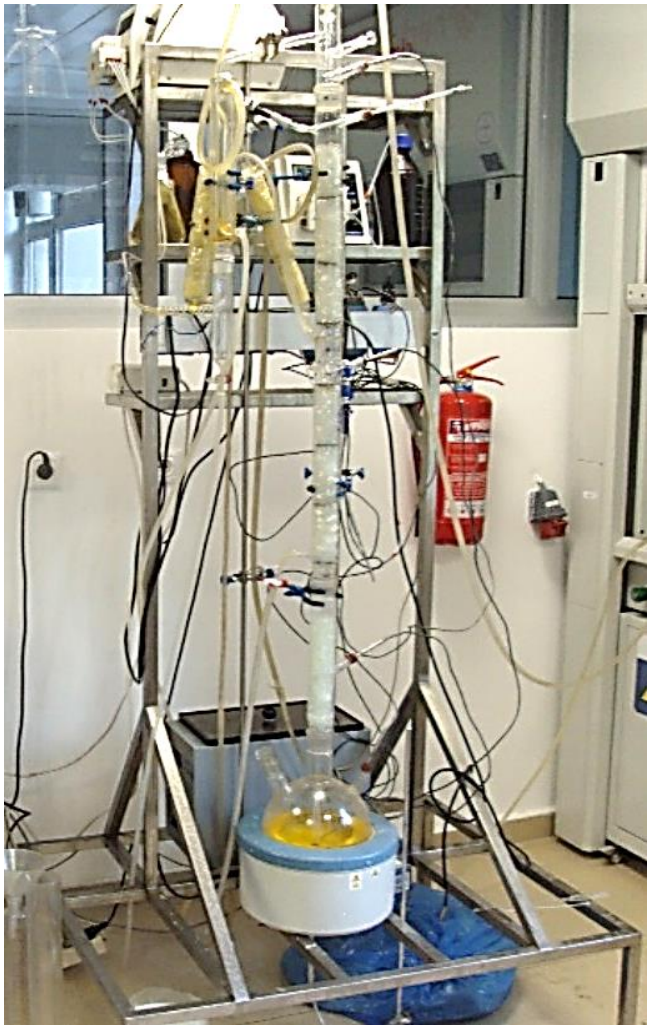

Figure 1. Pictorial view of packed RD column

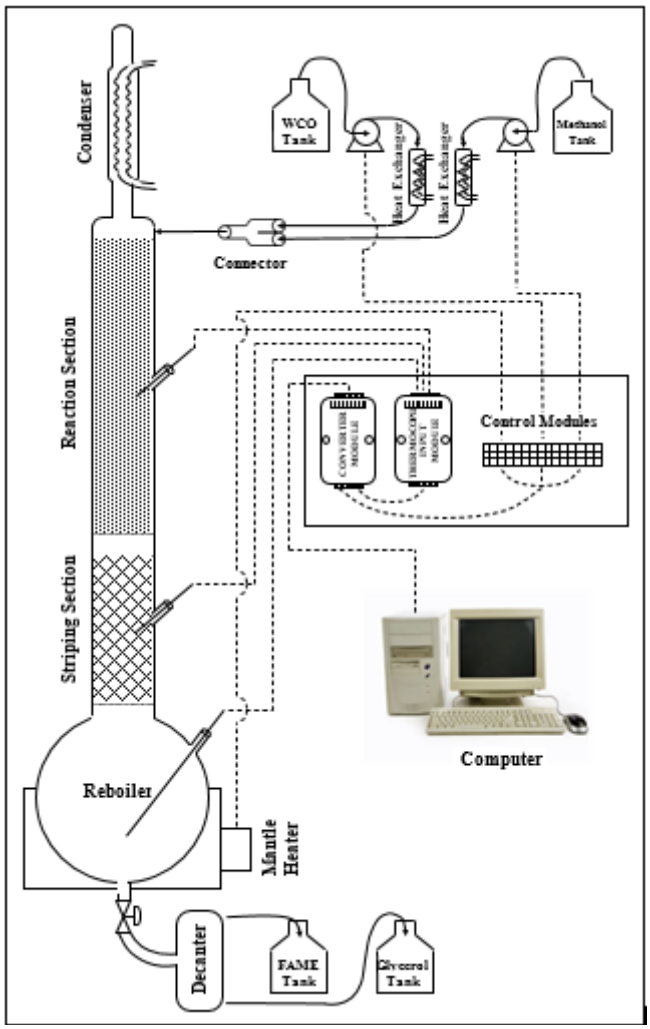

Figure 2. Sketch view of packed RD column

2.2. Kinetics Model

The overall vegetable oil methanolysis reaction could be presented by the following equation,

$$TG + 3\ ROH \leftrightarrow 3\ R'CO_2R + GL \quad (1)$$

and the intermediate reaction steps are;

$$TG + ROH \leftrightarrow DG + R'CO_2R \quad (2)$$

$$DG + ROH \leftrightarrow MG + R'CO_2R \quad (3)$$

$$MG + ROH \leftrightarrow GL + R'CO_2R \quad (4)$$

where, TG is triglyceride, DG is diglyceride, MG is monoglyceride, ROH is methanol, GL is glycerol and R'CO_2R is methyl ester. The heterogeneously catalyzed reaction is very complex due to happening in a three–phase system consisting of a solid catalysis and two immiscible oil and methanol phases. There are also some side reactions, such as saponification of glycerides and methyl esters, and neutralization of free fatty acids with the catalyst. Assuming the transesterification one–step reaction, the rate law could be expressed as one–way forward reaction as in Eq. 5 (Vujicic et al. 2010).

$$-r_a = -\frac{d[TG]}{dt} = k'\,[TG]\,[ROH]^3 \quad (5)$$

In Eq. (5), [TG] is the concentration of triglycerides, [ROH] is concentration of methanol and k' is the equilibrium rate constant. This overall reaction follows a second order reaction rate law. However, due to the high molar ratio of methanol to oil, the change in methanol concentration could be presumed ignorable, and the concentration can be considered as constant during the reaction. So, by taking excess methanol, it can be assumed that the reaction behaves like a first–order chemical reaction. Accordingly, the reaction obeys pseudo–first order kinetics and the rate expression can be written as,

$$-r_a = -\frac{d[TG]}{dt} = k\,[TG] \quad (6)$$

where k is modified rate constant and $k = k'.[ROH]^3$.

$$k = A_0\, e^{(-E_a/RT)} \quad (7)$$

The activation energy of reaction could be calculated by using Arrhenius equation (Eq. (7)). The slope and intercept of the graph of lnk vs 1/T gives the activation energy (E_a) and frequency factor (A_0). Birla et al. (2012) used calcined snail shell (CaO) catalyst to produce biodiesel from WCO and investigated the kinetic parameters. The activation energy and frequency factor of waste frying oil were determined as 79 kj/mol and 2.98×10^{10} min^{-1}, respectively.

2.3. Generalized Predictive Control Law

The GPC method was proposed by Clarke et al. (1987) and become one of the most popular MPC methods in industry and academia. It has been successfully applied in many industrial applications with good performance and a certain degree of robustness. This algorithm preserves steady control of processes with variable dead time and instantaneously changing model order providing the sufficient input/output data to allow reasonable process description. It is also effective with the non–minimum phase and open–loop unstable system where the model is over–parameterized, without taking special measures for the prediction method. The basic GPC scheme for nonlinear system can be seen in Fig. 3. It consists of a plant to be controlled, a nonlinear model and the Cost Function Minimization algorithm verifying the input required to produce the desired performance of that plant.

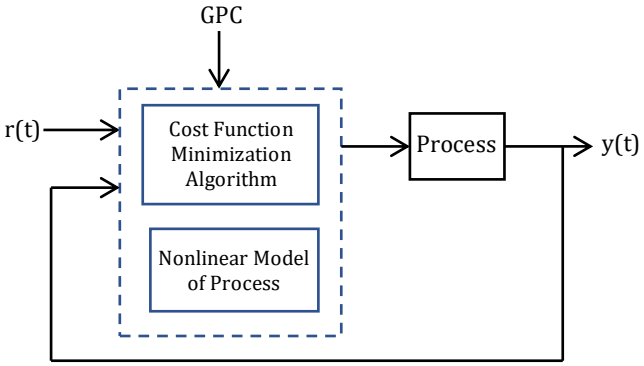

Figure 3. Basic structure of nonlinear GPC

GPC assumes an ARIMAX model for linear systems. The ARIMAX model describing the process in discrete–time GPC design is shown in Eq. (8).

$$A(z^{-1})\,y(t) = B(z^{-1})\,u(t-1) + \frac{C}{\Delta}\,e(t) \tag{8}$$

where,

$$A(z^{-1}) = 1 + a_1\,z^{-1} + \ldots\ldots\ldots + a_{na}\,z^{-na} \tag{9}$$

$$B(z^{-1}) = b_0 + b_1\,z^{-1} + \ldots\ldots\ldots + b_{nb}\,z^{-nb} \tag{10}$$

$$C(z^{-1}) = 1 + c_1\,z^{-1} + \ldots\ldots\ldots + c_{nc}\,z^{-nc} \tag{11}$$

The NARIMAX model is used in nonlinear (NL) GPC design. In this study, the exponential input term, $u(t)^m$, was used to describe the nonlinearity. So, the NARIMAX model could be given as follows,

$$y(t) = \frac{B}{A}u^m(t-1) + \frac{C}{A\Delta}e(t) \tag{12}$$

where difference operator expressed as $\Delta = (1 - z^{-1})$. While making GPC design, the cost function given in Eq. (13) is tuned to minimize its value.

$$J(N_1, N_2, N_u) = E\left\{\sum_{j=N_1}^{N_2}[y(t+j) - r(t+j)]^2 + \lambda\sum_{j=1}^{N_u}[\Delta u^m(t+j-1)]^2\right\} \tag{13}$$

where,

N_1	: Minimum costing prediction horizon
N_2	: Maximum costing prediction horizon
N_u	: Length of control horizon
$y(t+j)$	: Predicted output
$u(t)$	: Manipulated input
$r(t)$	: Reference trajectory
λ	: Weighing factor, lambda

To solve this minimization problem, it is necessary to make predictions beyond the j steps ahead based on the future and instantaneous values of the control increment. The estimation procedure involves the application of "Diophantine Equations" obtained from the NARIMAX model of the process. For the last term in Eq. (12), Diophantine Equation for step–forward forecast can be written as follows.

$$C = E_jA\Delta + z^{-j}F_j \tag{14}$$

where E_j and F_j are polynomials and are defined as,

$$E_j = 1 + e_1z^{-1} + \cdots + e_{j-1}\,z^{-j+1} \tag{15}$$

$$F_j = f_0 + f_1z^{-1} + \cdots + f_{j-1}\,z^{-j+1} \tag{16}$$

If Eqs. (14)–(16) are placed in Eq. (12) and rearranged,

$$y(t+j) = \frac{F_j}{C}y(t) + \frac{E_jB}{C}\Delta u^m(t+j-1) + E_je(t+j) \tag{17}$$

Eq. (17), where the last term represents the future charges, is achieved. It can be rewritten as follows,

$$y(t+j) = \frac{F_j}{C}y(t) + \frac{E_jB}{C}\Delta u^m(t+j-1) \tag{18}$$

Since Eq. (18) comprises future and past input data, a new Diophantine Equation (Eq. (19)) for the last term is defined to separate them.

$$\frac{E_jB}{C} = G_j + z^{-j}\frac{H_j}{C} \tag{19}$$

where H_j and G_j are polynomials and are defined as,

$$H_j = h_0 + h_1z^{-1} + \cdots + h_{j-1}\,z^{-j+1} \tag{20}$$

$$G_j = g_0 + g_1z^{-1} + \cdots + g_{j-1}\,z^{-j+1} \tag{21}$$

When Eqs. (18)–(21) are combined,

$$\bar{y}(t+j) = G_j\Delta u^m(t+j-1) + \frac{H_j}{C}\Delta u^m(t-1) + \frac{F_j}{C}y(t) \tag{22}$$

Eq. (22) is found. The last two terms in the equation represent the free response of the process. Thus, the predicted output of temperature response at j step ahead for the single–input single–output (SISO) NLGPC process can be given as,

$$\bar{y}(t+j) = G_j\Delta u^m(t+j-1) + f_j \tag{23}$$

Once Eq. (23) is located at the cost function (Eq. (13)), in the vector form, Eq. (24) is achieved.

$$J(N_1, N_2, N_u) = (\bar{y} - r)^2 + \lambda(\Delta u^m)^2 \quad (24)$$

If the steps are carried out and reorganized,

$$\begin{aligned} J(N_1, N_2, N_u) = {} & (G\,\Delta u^m)^T (G\,\Delta u^m) \\ & + (G\,\Delta u^m)^T (f - r) \\ & + (f - r)^T (G\,\Delta u^m) \\ & + (f - r)^T (f - r) \\ & + \lambda (\Delta u^m)^T \Delta u^m \end{aligned} \quad (25)$$

Eq. (25) is obtained. In terms of minimizing the cost function, the equation is derived and equated to zero. Reordering it, Eq. (26) has been found.

$$(G^T G + \lambda I)\,(\Delta u^m)^T + (f - r)^T G = 0 \quad (26)$$

Modifying Eq. (26), the future input data at step j can be calculated using Eq. (27) and (28).

$$\Delta u^m = (G^T G + \lambda I)^{-1}\, G^T (r - f) \quad (27)$$

$$u^m(t) = u^m(t-1) + (G^T G + \lambda I)^{-1}\, G^T (r - f) \quad (28)$$

Thus, SISO NLGPC algorithm will be fulfilled via control law, Eq. (27) and (28). The first element of the Δu^m vector, including predicted (t+j) solutions for the value of j from 1 to N_u, is applied to the process and temperature response is read from the process. Here, Eq. (23) is used to calculate the theoretical temperature response of the system for the next (t+1) th step by using the value of 1 of j. These periods are repeated cyclically in this way until the system response reaches the set value. During the procedure, the control gain remains constant and only the f and r vectors are calculated at each sampling time, repeatedly.

The block diagram developed to be used in system identification and experimental control studies, which will enable the application of manipulating variable values to the process, reading system temperatures, and recording all data automatically in a computer-controlled environment is as shown in Fig. 4.

2.4. Design of MIMO NLGPC

The reboiler temperature y_1 was controlled by the heat duty (Δu_1^m) manipulating variable. Likewise, the reaction temperature y_2 was controlled by the flow rate (Δu_2^m) manipulating variable at constant molar ratio.

2.4.1. Design of non–decoupled MIMO NLGPC

In non–decoupled MIMO NLGPC method, the SISO control law, Eq. (27), is written separately for reboiler and reaction sections, as seen in Eq. (29) and (30).

$$\Delta u_1^m = (G_{11}^T G_{11} + \lambda_1 I)^{-1}\, G_{11}^T\, (r_1 - f_{11}) \quad (29)$$

$$\Delta u_2^m = (G_{22}^T G_{22} + \lambda_2 I)^{-1}\, G_{22}^T\, (r_2 - f_{22}) \quad (30)$$

Solving these equations alone, the vectors Δu_1^m and Δu_2^m are found and using them, the future values of the manipulating variables, u_1^m and u_2^m, are attained. Accordingly, system responses are obtained by applying the first term of those to the process at time t. Here, the responses are calculated theoretically for the next (t+1) th step for the value of 1 of j through Eq. (31) and (32).

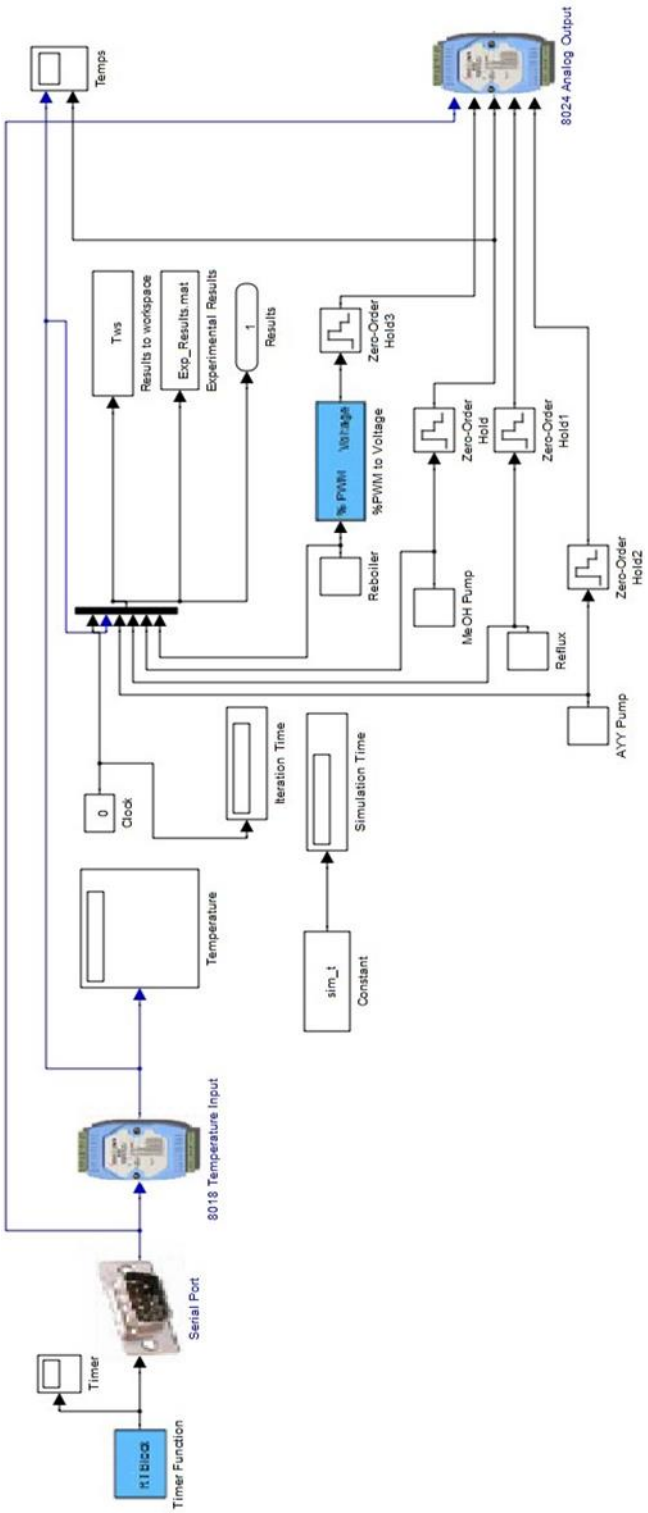

Figure 4. Block diagram for on–line control of process

$$\bar{y}_1(t+1) = G_{j,11}\Delta u_1^m(t) + f_{j,11} + G_{j,12}\Delta u_2^m(t) + f_{j,12} \quad (31)$$

$$\bar{y}_2(t+1) = G_{j,21}\Delta u_1^m(t) + f_{j,21} + G_{j,22}\Delta u_2^m(t) + f_{j,22} \quad (32)$$

Thus, the effect of both manipulating variables on both sides due to interaction is taken into account via Eq. (31) and (32) while calculating the system response of each region for the next control step. Repeating this period cyclically, process response is intended to reach the desired set values. The free response functions described in the equations are defined in Eq. (33).

$$
\begin{aligned}
f_{j,11} &= \frac{H_{j,11}}{C_{11}}\Delta u_1^m(t-1) + \frac{F_{j,11}}{C_{11}}y_{11}(t)\\
f_{j,12} &= \frac{H_{j,12}}{C_{12}}\Delta u_2^m(t-1) + \frac{F_{j,12}}{C_{12}}y_{12}(t)\\
f_{j,21} &= \frac{H_{j,21}}{C_{21}}\Delta u_1^m(t-1) + \frac{F_{j,21}}{C_{21}}y_{21}(t)\\
f_{j,22} &= \frac{H_{j,22}}{C_{22}}\Delta u_2^m(t-1) + \frac{F_{j,22}}{C_{22}}y_{22}(t)
\end{aligned}
\tag{33}
$$

2.4.2. Design of decoupled MIMO NLGPC

In the decoupled MIMO NLGPC method, the block diagram could be given as presented in Fig. 5.

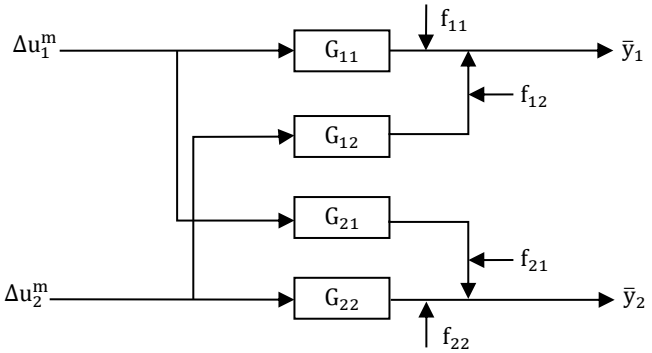

Figure 5. Decoupled MIMO NLGPC diagram

The predicted temperature responses of the reboiler and reaction sections at the j step ahead are defined as Eq. (34) and (35).

$$
\begin{aligned}
\bar{y}_1(t+j) = {} & G_{11}\Delta u_1^m(t+j-1) + f_{11}\\
& + G_{12}\Delta u_2^m(t+j-1) + f_{12}
\end{aligned}
\tag{34}
$$

$$
\begin{aligned}
\bar{y}_2(t+j) = {} & G_{21}\Delta u_1^m(t+j-1) + f_{21}\\
& + G_{22}\Delta u_2^m(t+j-1) + f_{22}
\end{aligned}
\tag{35}
$$

If the cost function is applied to Eq. (34) and (35), Eq. (36) and (37) are achieved.

$$
\begin{aligned}
J_1(N_1,N_2,N_u) = {} & (G_{11}\,\Delta u_1^m(t+j-1)\\
& + G_{12}\,\Delta u_2^m(t+j-1)\\
& + f_{11} + f_{12} - r_1)^2\\
& + \lambda_1\left(\Delta u_1^m(t+j-1)\right)^2
\end{aligned}
\tag{36}
$$

$$
\begin{aligned}
J_2(N_1,N_2,N_u) = {} & (G_{21}\,\Delta u_1^m(t+j-1)\\
& + G_{22}\,\Delta u_2^m(t+j-1)\\
& + f_{21} + f_{22} - r_2)^2\\
& + \lambda_2\left(\Delta u_2^m(t+j-1)\right)^2
\end{aligned}
\tag{37}
$$

For minimization, if derivatives of them are taken separately depending on u_1^m and u_2^m, equated to zero and the adjustments are made, Eq. (38) and (39) are found.

$$
\begin{aligned}
& (G_{11}^T G_{11} + \lambda_1 I)\,\Delta u_1^m(t+j-1)\\
& \quad + (G_{11}^T G_{12})\,\Delta u_2^m(t+j-1)\\
& \quad = G_{11}^T(r_1 - f_{11} - f_{12})
\end{aligned}
\tag{38}
$$

$$
\begin{aligned}
& (G_{22}^T G_{21})\,\Delta u_1^m(t+j-1)\\
& \quad + (G_{22}^T G_{22} + \lambda_2 I)\,\Delta u_2^m(t+j\\
& \quad - 1) = G_{22}^T(r_2 - f_{21} - f_{22})
\end{aligned}
\tag{39}
$$

To obtain predicted vectors, Δu_1^m and Δu_2^m, a matrix solution is made simultaneously using Eq. (38) and (39).

$$
\begin{aligned}
\Phi_1 &= G_{11}^T G_{11} + \lambda_1 I\\
\Phi_2 &= G_{11}^T G_{12}\\
\Phi_3 &= G_{22}^T G_{21}\\
\Phi_4 &= G_{22}^T G_{22} + \lambda_2 I
\end{aligned}
\tag{40}
$$

If the definitions, Eq. (40) and (41), are put in Eq. (38) and (39), matrix solution form, Eq. (42), is attained.

$$
\begin{aligned}
\Gamma_1 &= G_{11}^T(r_1 - f_{11} - f_{12})\\
\Gamma_2 &= G_{22}^T(r_2 - f_{21} - f_{22})
\end{aligned}
\tag{41}
$$

The solution algorithm was developed in MATLAB environment and the vectors, Δu_1^m and Δu_2^m, were acquired by multiplying the right–side matrix by the inverse of the coefficient matrix. Then, using them, u_1^m and u_2^m input values were calculated and the first terms of them were applied to the process. As in the non–decoupled MIMO NLGPC, the responses are calculated theoretically for the next (t+1) th step for the value of 1 of j via Eq. (31) and (32). Likewise, repeating the cycle periodically, the process responses are intended to reach the desired set values.

$$
\begin{bmatrix} \Phi_1 & \Phi_2 \\ \Phi_3 & \Phi_4 \end{bmatrix}
\begin{bmatrix} \Delta u_1^m(t+j-1) \\ \Delta u_2^m(t+j-1) \end{bmatrix}
= \begin{bmatrix} \Gamma_1 \\ \Gamma_2 \end{bmatrix}
\tag{42}
$$

2.5. Discrete–time PID Control Law

Typically, in the PID control systems, the input to be applied to the process is calculated by Eq. (43) including proportional, integral, and derivative impact. Its magnitude depends on the error which is difference between the process output and the set value at time t.

$$
\Delta u = K_c\left\{\varepsilon(t) + \frac{1}{\tau_I}\int_0^t \varepsilon(t)d(t) + \tau_D\frac{d\varepsilon(t)}{dt}\right\}
\tag{43}
$$

From the mathematical definitions of integral and derivative, Eq. (44) is obtained for the (n)th step.

$$
\begin{aligned}
u_n = u_0 + K_c\Bigg\{ & \varepsilon_n(t)\\
& + \frac{\Delta t}{\tau_I}\sum_{k=0}^{n}\varepsilon_k(t) + \frac{\tau_D}{\Delta t}\left(\varepsilon_n(t)\right.\\
& \left. - \varepsilon_{n-1}(t)\right)\Bigg\}
\end{aligned}
\tag{44}
$$

Next, if Eq. (44) is rewritten for the (n–1)th step and subtracted from the developed for the (n)th step, Eq. (45) and (46) are found in terms of the operator, z^{-j}.

$$
\begin{aligned}
\Delta u = {} & K_c\left(1 + \frac{\Delta t}{\tau_I} + \frac{\tau_D}{\Delta t}\right)\varepsilon_n\\
& - K_c\left(1 + \frac{2\tau_D}{\Delta t}\right)\varepsilon_n z^{-1}\\
& + K_c\frac{\tau_D}{\Delta t}\varepsilon_n z^{-2}
\end{aligned}
\tag{45}
$$

$$\frac{\Delta u(z)}{\varepsilon_n(z)} = K_c\left\{\left(1+\frac{\Delta t}{\tau_I}+\frac{\tau_D}{\Delta t}\right)-\left(1+\frac{2\tau_D}{\Delta t}\right)z^{-1}+\left(\frac{\tau_D}{\Delta t}\right)z^{-2}\right\} \quad (46)$$

Here, a new polynomial, S, is defined by Eq. (47).

$$S = s_0 + s_1 z^{-1} + s_2 z^{-2} \quad (47)$$

where,

$$s_0 = K_c\left(1+\frac{\Delta t}{\tau_I}+\frac{\tau_D}{\Delta t}\right)$$

$$s_1 = K_c\left(1+\frac{2\tau_D}{\Delta t}\right) \quad (48)$$

$$s_2 = K_c\left(\frac{\tau_D}{\Delta t}\right)$$

As mentioned before, the error, Eq. (49), is defined as the difference between the set value and the output in the PID control. If Eqs. (46)–(49) is restructured, the control law, Eq. (50), is attained for discrete–time SISO PID control application.

$$\varepsilon(z) = [r(t) - y(t)] \quad (49)$$

$$u(t) = \frac{S}{\Delta}[r(t) - y(t)] \quad (50)$$

2.6. Design of Discrete–time MIMO PID Control

In discrete–time PID control design, the process was stated in linear ARX model as shown in Eq. (51) and (52).

$$y(t) = \frac{B(z^{-1})}{A(z^{-1})}u(t-1) \quad (51)$$

$$y(t) = G(z^{-1})\,u(t-1) \quad (52)$$

2.6.1. Non–decoupled MIMO PID control

The discrete–time, interactive and non–decoupled MIMO PID control system is demonstrated as in Fig. 6.

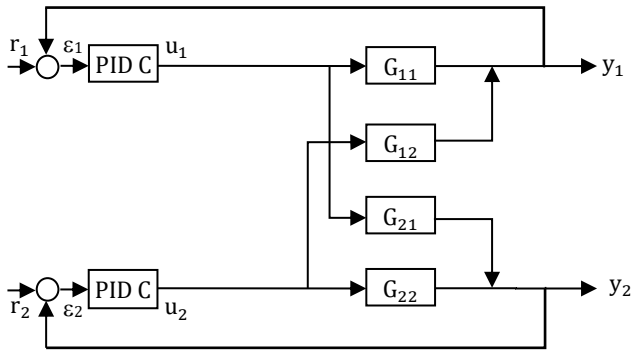

Figure 6. Non–decoupled MIMO PID control diagram

Process temperature responses y_1 and y_2 at time t are defined as in Eq. (53) and (54) in the non–decoupled MIMO PID system.

$$y_1(t) = G_{11}(z^{-1})u_1(t-1) + G_{12}(z^{-1})u_2(t-1) \quad (53)$$

$$y_2(t) = G_{21}(z^{-1})u_1(t-1) + G_{22}(z^{-1})u_2(t-1) \quad (54)$$

If discrete–time SISO PID control law, Eq. (50), is applied singly at each region Eq. (55) and (56) are gotten.

$$u_1(t) = \frac{S_1}{\Delta}\,[r_1(t) - y_1(t)] \quad (55)$$

$$u_2(t) = \frac{S_2}{\Delta}\,[r_2(t) - y_2(t)] \quad (56)$$

Then, calculated manipulating variables are applied to the process. Here, the interacted process responses are computed theoretically for the next (t+1) th step by Eq. (53) and (54) by using manipulating variable values achieved at time t. In this way, the cycle is continued repeatedly until reaching the desired set values.

2.6.2. Decoupled MIMO PID control

The discrete–time, interactive and decoupled MIMO PID control system is presented as in Fig. 7. In control scheme, the process temperature output y_1 and y_2 at time t will be as given by Eq. (57) and (58).

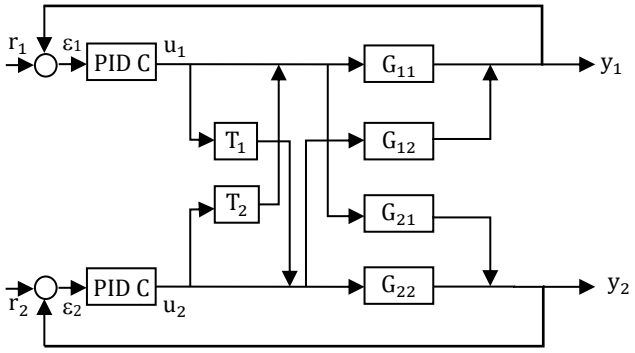

Figure 7. Decoupled MIMO PID control diagram

$$y_1(t) = G_{11}(z^{-1})[u_1(t-1) + T_2u_2(t-1)] + G_{12}(z^{-1})[u_2(t-1) + T_1u_1(t-1)] \quad (57)$$

$$y_2(t) = G_{22}(z^{-1})[u_2(t-1) + T_1u_1(t-1)] + G_{21}(z^{-1})[u_1(t-1) + T_2u_2(t-1)] \quad (58)$$

Eq. (59) and (60) are found if adjustments are made.

$$y_1(t) = [G_{11}(z^{-1}) + G_{12}(z^{-1})\,T_1]\,u_1(t-1) + [G_{12}(z^{-1}) + G_{11}(z^{-1})\,T_2]\,u_2(t-1) \quad (59)$$

$$y_2(t) = [G_{21}(z^{-1}) + G_{22}(z^{-1})\,T_1]\,u_1(t-1) + [G_{22}(z^{-1}) + G_{21}(z^{-1})\,T_2]\,u_2(t-1) \quad (60)$$

When the terms including u_1 in Eq. (60) and u_2 in Eq. (59) are equated to zero, Eq. (61) is acquired.

$$T_1 = -[G_{21}(z^{-1}) / G_{22}(z^{-1})]$$

$$T_2 = -[G_{12}(z^{-1}) / G_{11}(z^{-1})] \quad (61)$$

In the control, initially, process inputs u_1 and u_2 are calculated by the control laws, Eq. (55) and (56), at time t. Then revised inputs, $\{u_1(t)–[u_2(t)G_{12}(z^{-1})/G_{11}(z^{-1})]\}$ and $\{u_2(t)–[u_1(t)(G_{21}(z^{-1})/G_{22}(z^{-1})]\}$, are applied to process. Once again, Eq. (53) and (54) are used to get theoretical responses for the next (t+1) th step as mentioned above.

3. RESULTS

This section describes our experience in applying multivariate NLGPC and discrete–time PID control of the packed RD column. The aim of the control study is to keep the temperatures of reaction and reboiler sections at the desired set value during the reaction taken place in the column. This goal was achieved by changing the feed flow rate at constant molar ratio and reboiler heat duty.

3.1. System Identification Outcomes

The parameters of NARIMAX and ARX models were ascertained experimentally. First, PRBS impacts were given to the process. Next, the temperature responses of reaction and reboiler sections for each PRBS effect were measured individually. The PRBS effect of WCO flow rate (Fig. 8a) was applied at 350 watts reboiler heat duty and 1.8–4.0 ml/min WCO flow rate range with constant 8.19 molar ratio. Likewise, the PRBS effect of reboiler heat duty (Fig. 8b) was implemented to the process at 4.0 ml/min WCO flow rate with constant molar ratio of 8.19 and 280–420 watt reboiler heat duty range.

After application of WCO flow rate and heat duty PRBS effects to the process separately, the temperature responses were obtained experimentally and used in defining the parameters of the models. To do so, two separate ".m" files, containing the "rarmax" tool created in MATLAB for use in ARMAX models but with the intention of using in NLGPC and the "arx" tool developed in MATLAB for use in ARX models employed in discrete-time PID controls, were formed in MATLAB environment.

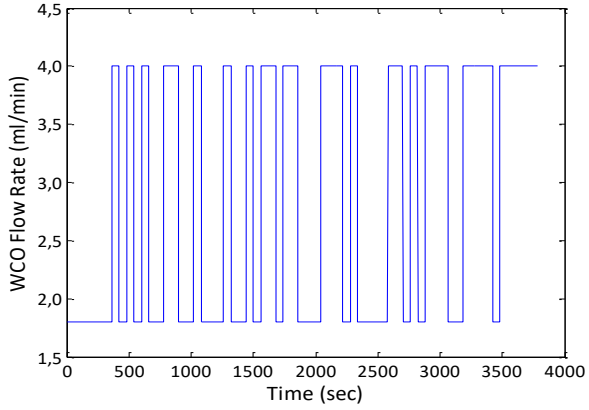

(a)

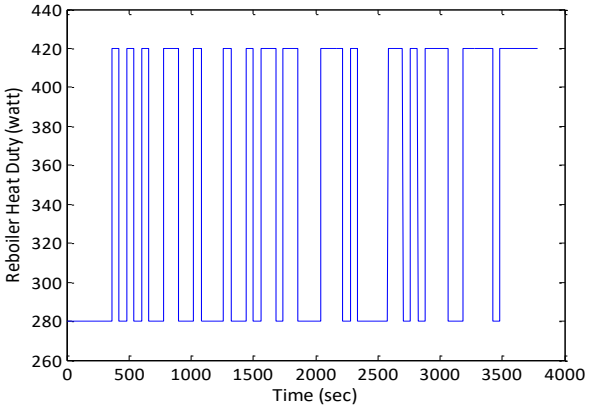

(b)

Figure 8. PRBS effect, (a) WCO flow rate with constant MR=8.19 (Q=350 watt), (b) Heat duty (F_{WCO}=4.0 ml/min)

On account of the "rarmax" tool has been used for the ARMAX model in MATLAB application, in the study, the use of ΔA and ΔB polynomials was taken as a basis instead of A and B to be able to use this command for the ARIMAX model with integral effect. Polynomial degrees of n_ΔA, n_ΔB, nc and nk for ARIMAX models and na, nb and nk for ARX models, given in the Table 2 and 4, were ascertained by regression method based on comparison of the theoretical temperature outputs gotten from the models for the different values of these parameters with the temperature responses achieved experimentally.

Table 2. Exponential, degree and IAE, ISE values of NARİMAX models

	G_{11}	G_{21}	G_{12}	G_{22}
m	8	8	4	4
n_ΔA	4	5	3	3
n_ΔB	3	4	3	3
nc	1	1	1	1
nk	1	1	1	1
IAE	3.9464	9.4072	1.5658	4.1056
ISE	0.0386	0.0461	0.0154	0.0097

Table 3. Polynomial coefficients of NARİMAX models

G_{11}	ΔA_{11}	[1.0000 −0.9572 −0.0279 0.0143 −0.0293]
	$\Delta B_{11} *10^{6}$	[−0.2219 0.6929 −0.4685]
	C_{11}	[1.0000 −0.6232]
G_{21}	ΔA_{21}	[1.0000 −0.8929 −0.1112 0.0119 −0.0308 0.0231]
	$\Delta B_{21} *10^{6}$	[−0.0144 0.3466 −0.4639 0.1291]
	C_{21}	[1.0000 −0.5114]
G_{12}	ΔA_{12}	[1.0000 −0.9933 −0.0064 −0.0003]
	$\Delta B_{12} *10^{11}$	[−0.0455 0.1221 −0.0754]
	C_{12}	[1.0000 −0.6435]
G_{22}	ΔA_{22}	[1.0000 −0.9915 −0.0270 0.0186]
	$\Delta B_{22} *10^{12}$	[0.1414 −0.5421 0.4637]
	C_{22}	[1.0000 −0.4701]

Table 4. Degree and IAE, ISE values of ARX models

	G_{11}	G_{21}	G_{12}	G_{22}
na	4	5	3	3
nb	3	4	3	3
nk	1	1	1	1
IAE	27.8004	24.7444	25.9701	26.3009
ISE	0.3280	0.2599	0.3010	0.2975

Table 5. Polynomial coefficients of ARX models

G_{11}	A_{11}	[1.0000 −0.4059 −0.2698 −0.1929 −0.1314]
	B_{11}	[−0.0018 0.0040 −0.0024]
G_{21}	A_{21}	[1.0000 −0.4981 −0.3018 −0.1489 −0.0821 0.0308]
	$B_{21} * 10^{3}$	[−0.0347 0.0164 −0.3535 0.2235]
G_{12}	A_{12}	[1.0000 −0.4412 −0.3055 −0.2533]
	$B_{12} * 10^{4}$	[−0.0816 0.1540 −0.0679]
G_{22}	A_{22}	[1.0000 −0.4491 −0.3439 −0.2070]
	$B_{22} * 10^{4}$	[0.4864 −0.3771 −0.1044]

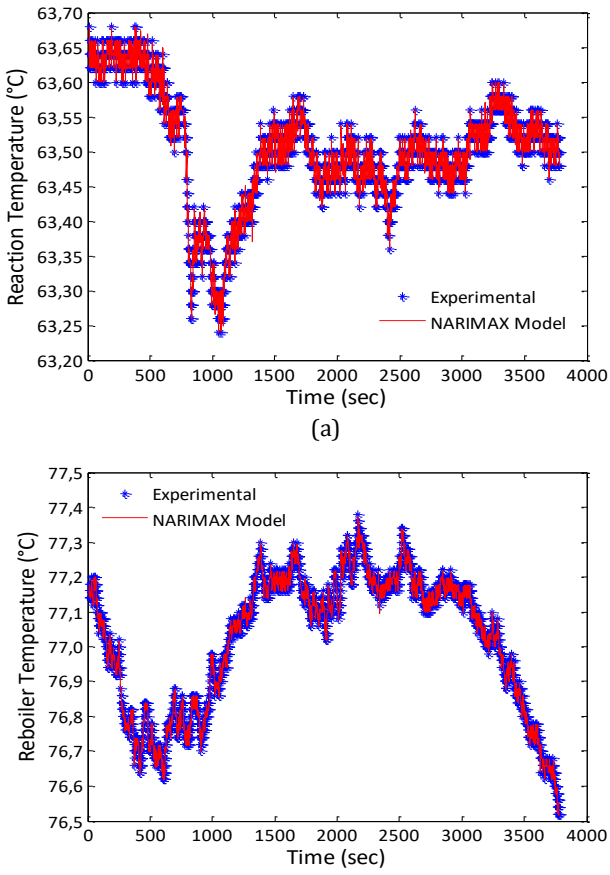

Figure 9. Temperature responses in WCO flow PRBS effect and curve fittings of NARIMAX models

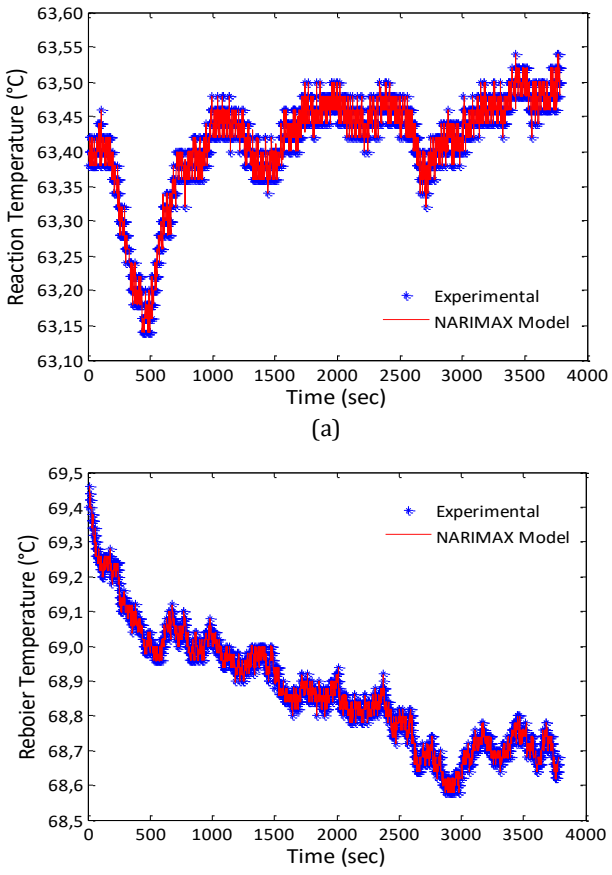

Figure 10. Temperature responses in reboiler heat duty PRBS effect and curve fittings of NARIMAX models

In regression method, the most suitable degree of parameters, presented in Table 2 and 4, were established with the help of curve fitting of models with the experimental data via assessing the sum of absolute value of error (IAE) and squares of error (ISE) given in Table 2 and 4. Relating to the polynomial coefficients, discrete–time PID ones, stated at Table 5, were obtained from the accepted solution iteration step for degree of parameters with the help of "arx" tools. As for the polynomial coefficients of NARIMAX models, additional calculations in the same manner were repeated at the different exponential, m, values of the manipulating variables. Accordingly, the most appropriate m value, where the best fit of the theoretical output and experimental temperatures was achieved depending on IAE and ISE shown in Table 2, and related coefficients presented at Table 3, were taken as the solution with the help of "rarmax" tools, as stated above. Experimental temperature responses and model outputs for reaction and reboiler sections were exhibited in Fig. 9 and 10.

3.2. Theoretical Control with MIMO NLGPC

In the control studies with NLGPC, firstly, Gj polynomials used in the equations in which the value of future time manipulating variable and temperature responses for j th step were calculated were obtained. For this purpose, with the first Diophantine Equation, Eq. (14), the C polynomial was divided into ΔA polynomial. In other words, to obtain the Ej polynomial at the j th step, division process was continued till j th step number. Thus, at the end of the division at each the j th step, the Ej polynomial from the coefficients of the quotient and the Fj polynomial used in the f free response vector from the coefficients of the remainder were obtained. Then, with the help of the second Diophantine Equation, Eq. (19), at each j th step, Ej polynomial with j th step size and B polynomial was multiplied and divided by C polynomial till the j th step size. Likewise, at the end of the division at each j th step, the Gj polynomial from the coefficients of the quotient, the Hj polynomial used in the f free response vector from the coefficients of the remainder and the jxj size G matrix containing Gj polynomials were obtained. To carry out these processes autonomously, algorithms containing necessary codes were developed in MATLAB and with the help of the programs embedded in the control algorithms, Ej, Fj, Gj and Hj polynomials could be easily calculated and Gj,j matrix can be created from Gj by the computer during the control mechanism.

In the NLGPC design, N_1, N_2 and N_u were selected as 1, 20 and 20, respectively. Later, optimum value of lambda, λ, was determined depending on the response time, error value and oscillation in reaching to the set temperature through the non–decoupled and decoupled MIMO NLGPC algorithms developed for control action. In the literature, the 2nd, 3rd, and 4th powers of the manipulated variable were used in the control studies with the NLGPC method using the NARIMAX model (Hapoğlu et al. 2000; Karacan 2003; Özkan et al. 2006; Zeybek et al. 2006). Additionally, a control study was examined using exponential value of 0.8–2.2 and λ values of $1.4x10^{-12}$ – $9.0x10^{-16}$ (Hapoğlu 2002).

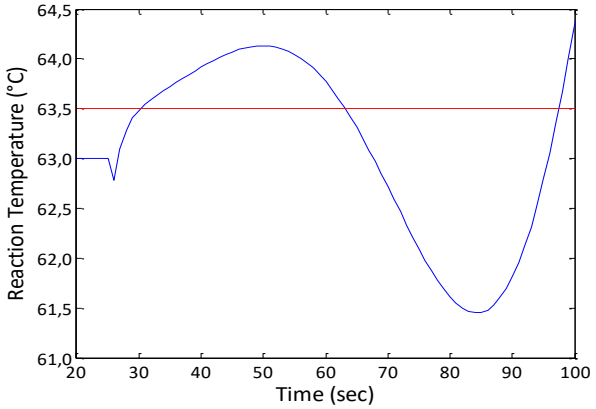

(a)

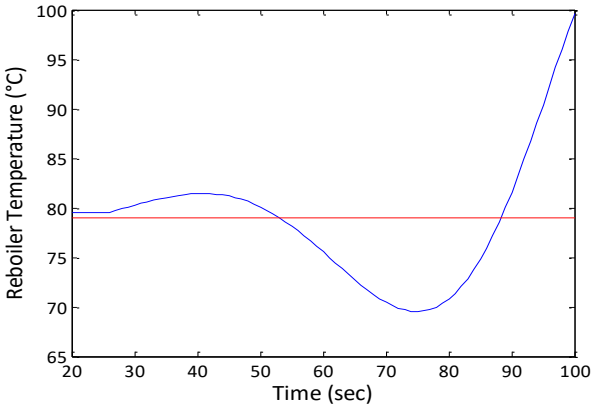

(b)

Figure 11. Temperature responses in non–decoupled MIMO NLGPC (T_rxn_sp = 63.5 °C, T_reb_sp = 79.0 °C)

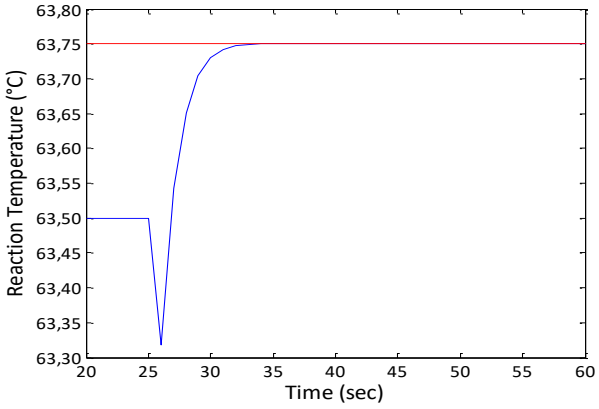

(a)

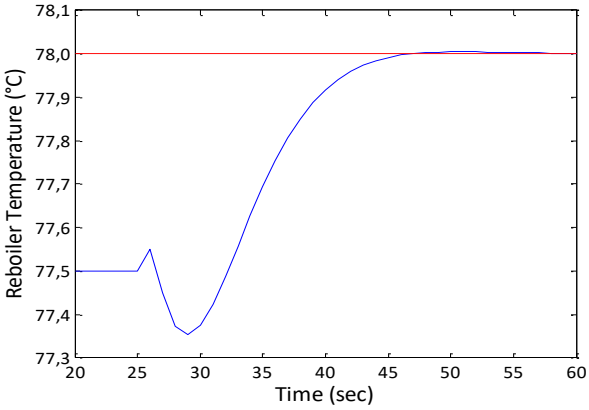

(b)

Figure 13. Temperature responses in decoupled MIMO NLGPC (T_rxn_sp = 63.75 °C, T_reb_sp = 78.0 °C)

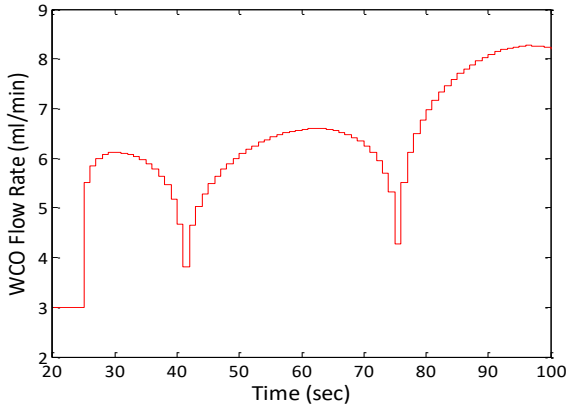

(a)

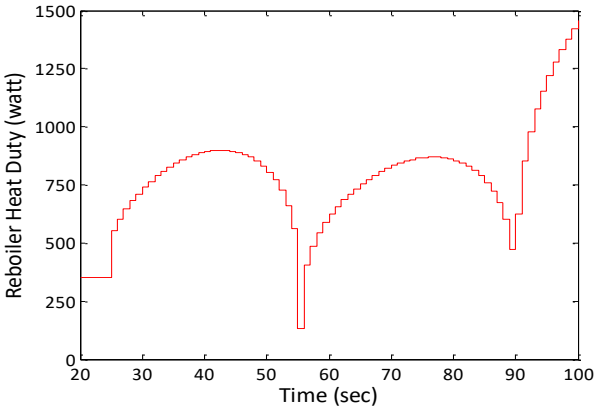

(b)

Figure 12. Changing of manipulating variables in non–decoupled MIMO NLGPC

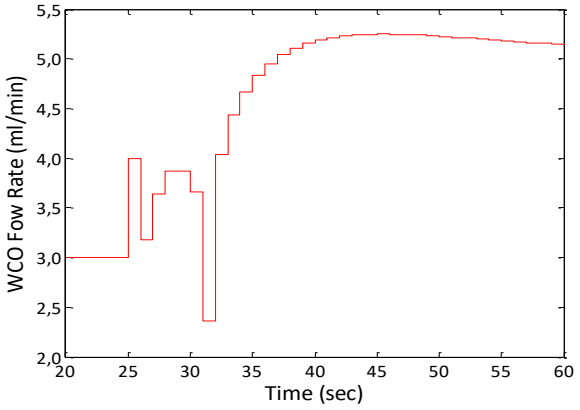

(a)

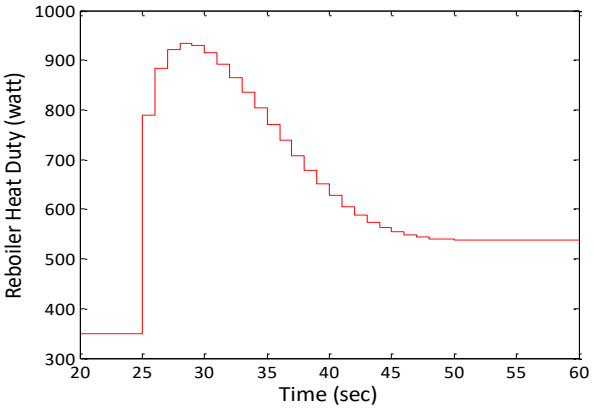

(b)

Figure 14. Changing of manipulating variables in decoupled MIMO NLGPC

Table 6. λ values of NLGPC algorithms

		λ values
Control with non–decoupled MIMO NLGPC	Reaction Section	1×10^{-13}
	Reboiler Section	1×10^{-27}
Control with decoupled MIMO NLGPC	Reaction Section	1×10^{-14}
	Reboiler Section	1×10^{-24}

In this study, λ values used in theoretical control with NLGPC were presented in Table 6. Accordingly, exponential values of 8 and 4, and λ values of 1.0×10^{-13} – 1.0×10^{-27} were used for the reaction and reboiler region, in turn.

Temperature responses and manipulating variables variations obtained in synchronized control of reaction and reboiler regions with non–decoupled MIMO NLGPC were presented in Fig. 11 and 12. It was noticed that the specified set values could not be reached.

Although it is not possible to control the reaction and reboiler region temperature simultaneously with non–decoupled MIMO NLGPC, it has been observed that the desired set values have been reached with decoupled MIMO NLGPC. Temperature responses and manipulating variable changes were given in Fig. 13 and 14.

3.3. Theoretical Control with MIMO PID Control

Initially, codes were formed in MATLAB for PID control algorithms. Parameters of gain factor (K_C), integral time (τ_I) and derivative time constant (τ_D) were ascertained depending on the magnitude of the error originating from the difference between temperature response and desired set value and oscillation frequency defining whether temperature response reaches the set value immediately or not. So, the most appropriate values were postulated and presented in Table 7.

It was observed that the desired set values were reached with both the non–decoupled and decoupled MIMO PID control in the simultaneous control of the reaction and reboiler regions.

Upon examined Fig. 14, 16 and 18, it was seen that the profiles of manipulating variables varied occasionally above or below operating ranges and sometimes in the negative region. It should be remembered that the signs and magnitudes of the coefficients of A, B and C polynomials presented in Table 3 and 5 were the values determined by PRBS effects of the manipulating variables at their definite ranges, with the effect of the interaction in the process. However, in the theoretical control studies, while the calculation of the magnitude of the manipulating variables to be applied to the process for the next control step were not restricted as minimum and maximum constraints specifying the operating range. Thus, some situations such as below or above the required limits and positive or negative values were encountered in line with the contribution of each related A and B polynomials depending on the sign and size of each coefficient of them to the temperature responses computed by Eq. (53) and (54) using the next control step value of manipulating variable for discrete-time PID control. Similarly, the effect of Gj and the free response parameter fj, including the polynomials Fj, Hj and C, on calculation of predicted manipulating variables by Eq. (29), (30) and (42) and, computing of the temperature responses by Eq. (31) and (32) are the same for NLGPC. If briefly explained as an example, the coefficients of the related B polynomial were multiplied with the related current and past time step value of manipulating variable and the products were summed. While doing this, calculation of temperature response of each region, it sometimes led to obtain and use the positive or negative value of manipulating variables to provide the response be able to reach the targeted set value as soon as possible.

Table 7. Control constants of PID algorithms

		K_C	τ_I	τ_D
Control with non–decoupled MIMO PID	Reaction Section	80	1850	1
	Reboiler Section	1000	1	1
Control with decoupled MIMO PID	Reaction Section	60	2150	1
	Reboiler Section	1000	1	1

It might be important to remember just here that, as mentioned before, in determining the control constants of discrete-time PID control and lambda for NLGPC, it was taken as a basis that the process response reached the set value in the shortest time with steeper slope without oscillation under the given set value without any restriction. Therefore, the program moved in this direction while calculating the manipulating variable for the next control step and evaluated the required value. Besides, it was also assessed that the magnitude and sign of set values applied simultaneously to both regions, and the interactions in the process were also influential in getting at this scale and size of manipulating variables and response time.

Moreover, it should not be overlooked that, with the software working in this way, the opportunity to compare the temperature responses were obtained without any intervention and restriction to the system. Namely, it was seen that how the software would work, and process response and the manipulating variable variation would–be under the same set value effect for both control algorithms. Accordingly, it was observed that although the process reached the set values in the range of positive and/or negative values of the manipulating variable in both algorithms, superiority of the NLGPC was obvious when the profiles of temperature response and manipulating variable were evaluated in terms of the rate of slope of the curve reaching to the set value, oscillation, and the scale and size of range of manipulating variables and the response time.

In the application of these algorithm in experimental control studies as they are, if the manipulating variable calculated in each control period for the next control step is outside the operating range, the maximum or minimum value of the operating range should be assigned to the manipulating variable and applied to the process for this control phase. Thus, each section could be intended to achieve the temperature set value cyclically within the range of manipulating variable.

4. DISCUSSION

Examining Table 2, 4, Fig. 9 and 10, in terms of compliance, NARİMAX models were found to represent the process fittingly in comparison to ARX models as for system identification.

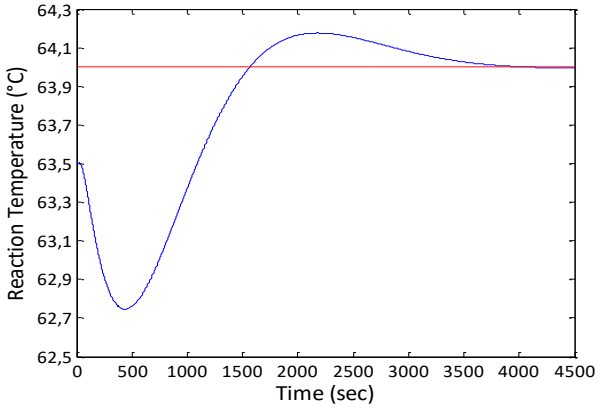

(a)

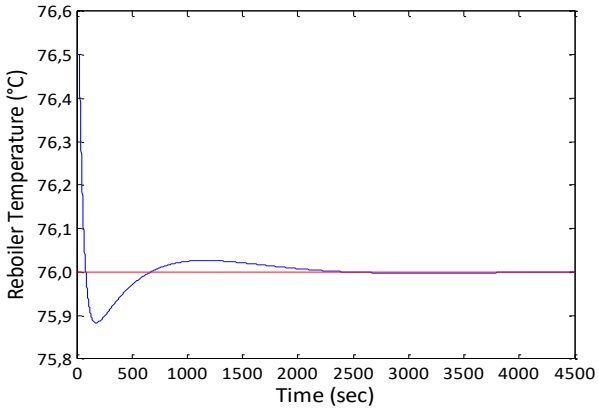

(b)

Figure 15. Temperature responses in non–decoupled MIMO PID control (T_rxn_sp=64.0 °C, T_reb_sp=76.0 °C)

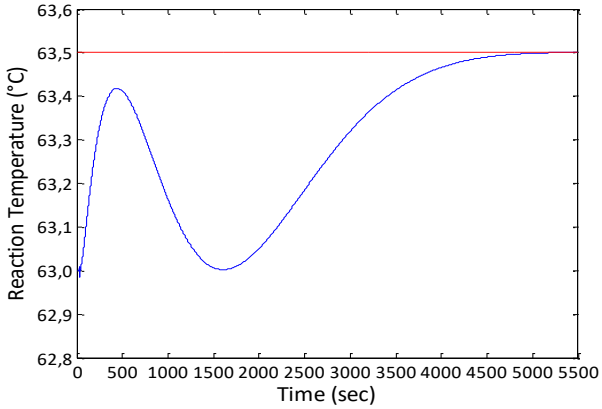

(a)

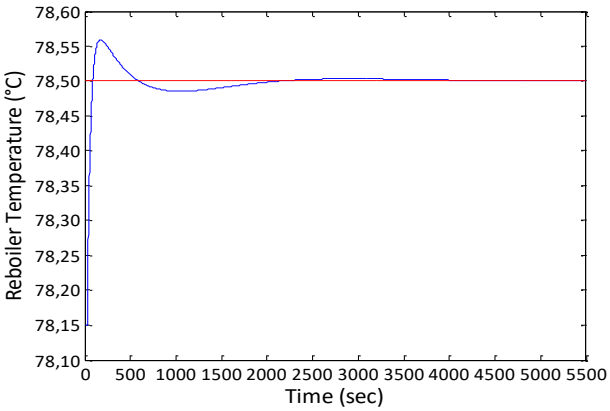

(b)

Figure 17. Temperature responses in decoupled MIMO PID control (T_rxn_sp = 63.5 °C, T_reb_sp = 78.5 °C)

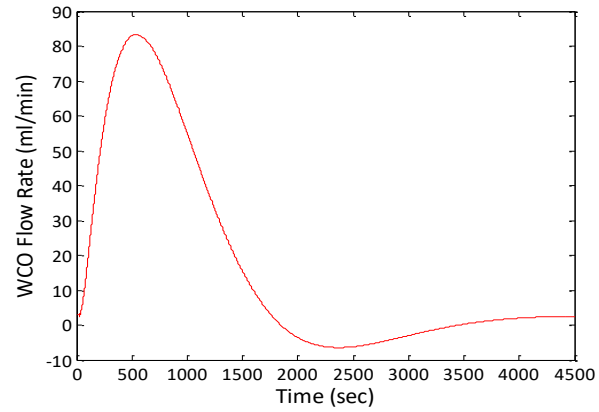

(a)

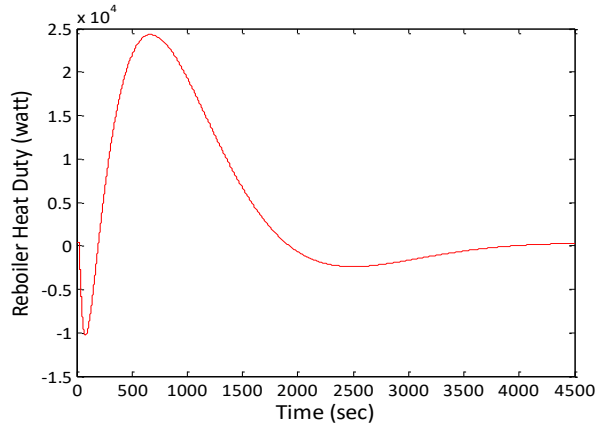

(b)

Figure 16. Changing of manipulating variables in non–decoupled MIMO PID control

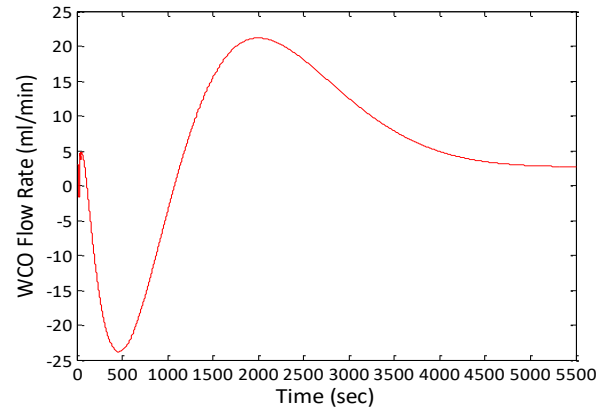

(a)

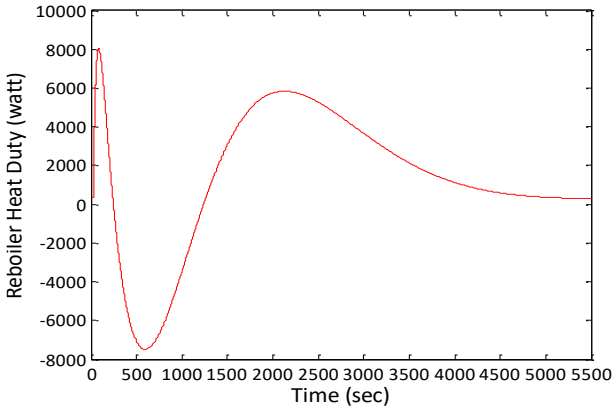

(b)

Figure 18. Changing of manipulating variables in decoupled MIMO PID control

Table 8. IAE and ISE values in theoretical MIMO control

Control Method	IAE		ISE	
	T_rxn	T_reb	T_rxn	T_reb
Non–decoupled MIMO NLGPC	2.22E+15	1.63E+16	9.12E+28	6.22E+30
Decoupled MIMO NLGPC	0.82	6.09	0.24	2.87
Non–decoupled MIMO PID Cont.	1348.10	74.74	1097.50	6.50
Decoupled MIMO PID Control	1082.50	41.66	382.19	2.35

Further, IAE and ISE values were calculated to compare the performances of non–decoupled and decoupled MIMO NLGPC and discrete–time PID control and presented in Table 8. With respect to PID control, it was seen that the gain constant is smaller, and the integral constant is larger in decoupled PID control compared to the non–decoupled one for the reaction side, if examined Table 7. This resulted in obtaining a lower value of manipulating variable than that of the non–decoupled one. Thus, it was ensured that the effects from reboiler to reaction side and from reaction to reboiler side due to the interaction were taken into account throughout the calculation of the manipulating variable. So, examining Fig. 15–18, it was seen that the profiles of temperature response and manipulating variable altered in a narrower range compared to the non–decoupled PID control, and thus, the error values presented in Table 8 were obtained smaller. Particularly, the lesser ISE value obtained for the decoupled PID control compared to the other one supported that the error values calculated in the control steps varied in a smaller range and resulted in a better control performance in comparison with the non–decoupled PID control. Finally, it was seen that theoretical control with non–decoupled MIMO NLGPC is not possible, but, owing to the smallest IAE and ISE in all control mechanisms, the obvious superiority of the control with decoupled MIMO NLGPC was revealed, if inspected Table 8 and Fig. 11–14.

5. CONCLUSION

In this study, we investigated multivariable control of CaO catalyst–packed RD column used for biodiesel production from WCO. For this aim, non–decoupled and decoupled MIMO NLGPC and discrete–time MIMO PID algorithms were utilized. At the beginning, system identification was performed for NARIMAX and ARX models via PRBS impacts. Subsequently, coefficients of model polynomials of A, B and C were determined by a parameter estimation technique. Later, those models were used in NLGPC and PID control algorithms.

The aim of the process control was to keep the temperatures of reaction and reboiler section at its set point. This goal was achieved by manipulating the feed flow rate with constant molar ratio and reboiler heat duty. Except for non–decoupled MIMO NLGPC, it has been seen that process control is well possible using control laws and codes developed for NLGPC and PID controls. Consequently, it should be noted that the decoupled MIMO NLGPC method is excellent with the best control results in all cases examined.

Author contributions

Mehmet Tuncay Çağatay: Conceptualization, Investigation, Methodology, Visualization, Software, Writing-Original draft preparation, Reviewing and Editing. **Süleyman Karacan:** Supervision, Validation, Writing-Reviewing and Editing.

Conflicts of interest

The authors declare no conflicts of interest.

REFERENCES

Ahn S M, Park M J & Rhee H K (1999). Extended Kalman filter–based nonlinear model predictive control for a continuous RIMA polymerization reactor. Ind. Eng. Chem. Res., 38 (10), 3942–3949.

Birla A, Singh B, Upadhyay S N & Sharma Y C (2012). Kinetics studies of synthesis of biodiesel from waste frying oil using a heterogeneous catalyst derived from snail shell. Bioresource Technol., 106, 95–100.

Chen W T & Xu C X (2001). Adaptive nonlinear control with partial overparameterization. Sys.Cont.Lett., 44, 13–24.

Clarke D W, Mohtadi C & Tuffs P S (1987). Generalized predictive control Part I, the basic algorithm. Automatica, 23(2), 137–148.

Clarke D W & Mohtadi C (1989). Pro wrties of Generalized Predictive Control. Automatica, 25, 137–160.

Çağatay M T & Karacan S (2018). Simulation and optimization of reactive packed distillation column for biodiesel production using heterogeneous catalyst. International Journal of Energy Applications and Technologies, 5(4), 153–160.

DiSerio M, Tesser R, Pengmei L & Santacesaria E (2008). Heterogeneous catalysts for biodiesel production. Energy Fuels, 22, 201–217.

Donato A G, Gonçalves J A, Peres J S, Ramos A L S, Ribeiro de Melo Jr A L D C A, Antunes O A C, Furtado N C & Taft C A (2009). The use of acids, niobium oxide, and zeolite catalysts for esterification reactions. J.Phys.Org.Chem, 22, 709–716.

Hapoğlu H, Özkan G & Alpbaz M (2000). Optimal temperature control in a batch polymerization reactor using Nonlinear Generalized Predictive Control. Chem. Eng. Commun., 183(1), 155–185.

Hapoğlu H (2002). Nonlinear Long-range Predictive Control of an openloop unstable reactor. Computers and Chemical Engineering, 26, 1427–1436.

Harmsen G J (2007). Reactive distillation: the frontrunner of industrial process intensification a full review of commercial applications, research, scale–up, design and operation. Chem. Eng. Process, 46, 774–780.

Karacan S (2003). Application of a nonlinear long-range predictive control to a packed distillation column. Chem. Eng. and Processing, 42(5), 943–953.

Kouzu M, Kasuno T, Tajika M, Sugimoto Y, Yamanaka S & Hidaka J (2008). Calcium oxide as a solid base catalyst for transesterification of soybean oil and its

application to biodiesel production. Fuel, 87, 2798–2806.
Kulkarni M G & Dalai A K (2006). Waste cooking oil – an economical source for biodiesel: a review. Ind. Eng. Chem. Res., 45, 2901–2913.
Martín M & Grossmann I E (2012). Simultaneous optimization and heat integration for biodiesel production from cooking oil and algae. Ind. Eng. Chem. Res, 51, 7998–8014.
Özkan G, Hapoğlu H & Alpbaz M (2006). Non–linear Generalised Predictive Control of a jacketed well mixed tank as applied to a batch process—A polymerisation reaction. Applied Thermal Engineering, 26, 720–726.
Sharma Y C, Singh B & Upadhyay S N (2008). Advancements in development and characterization of biodiesel. Fuel, 87, 2355–2373.
Srivastava A & Prasad R (2000). Triglycerides–based diesel fuels. Renew. Sustainable Energy Rev., 4, 111–133.
Vujicic D J, Comic D, Zarubica A, Micic R & Boskovi G (2010). Kinetics of biodiesel synthesis from sunflower oil over CaO heterogeneous catalyst. Fuel, 89, 2054–2061.
Zeybek Z, Çetinkaya S, Hapoğlu H & Alpbaz M (2006). Generalized delta rule (GDR) algorithm with generalized predictive control (GPC) for optimum temperature tracking of batch polymerization. Chemical Engineering Science, 61, 6691–6700.
Zhang Y, Dube M A, McLean D D & Kates M (2003). Biodiesel production from waste cooking oil: 1. Process design and technological assessment. Bioresource Technology, 89, 1–16.